Smart Geotechnics for Smart Societies – Zhussupbekov, Sarsembayeva & Kaliakin (Eds)

Computed and observed deformations of fill-type dams by strong earthquake

Tadatsugu Tanaka
The University of Tokyo, Japan

Hiroshi Mori
Faculty of Agriculture and Life Sciences, Hirosaki University, Japan

Kenji Okajima
Department of Environmental Science and Technology, Mie University, Japan

Askar Zh. Zhussupbekov
The Geotechnical Institute, L. N. Gumilyov Eurasian National University, Kazakhstan

ABSTRACT: An earthquake measuring 6.6 Mw struck southern Hokkaido, Japan, September 2018. Mizuho Dam and Azuma Dam were located near the epicenter of this earthquake and strongly shaken. The recorded base peak accelerations of Mizuho Dam in upstream and downstream directions was 491 gal and 937gal was recorded at dam crest. Maximum settlement of crest at upstream slope side was about 12cm and cracks attained about 2.0 m depth were observed around the crest. Azuma Dam's spillway was blocked by debris from landslides. Recorded base peak acceleration was 297 gal and 1293 gal was recorded at dam crest. A simple strain softening elasto-plastic constitutive model is applied to both dams with the features of non-associated flow characteristics, post-peak strain softening, and strain-localization into a shear band with a specific width. The dynamic response analyses of both dams and the computed settlements are compared to observed one.

1 INTRODUCTION

Mizuho Dam is a gravel-fill dam with central clay core zone shown in Figure 1 completed 1998. It is 25.9 m high and 427.05 m long, impounding up to 4,300,000 m^3 of water. Two seismometers were installed at the crest and the base ground as shown in Figure 1. An earthquake measuring 6.7 Mw on the moment magnitude scale struck Iburi Subprefecture in southern Hokkaido, Japan, on 6 September 2018. The earthquake's epicenter was near Azuma Town and occurred at a depth of around 33.0 km. Mizuho Dam located near the epicenter of this earthquake and strongly shaken. The recorded base peak acceleration of Mizuho Dam obtained by the seismometer in upstream and downstream direction was 491 Gal, and 937 Gal was recorded at the dam crest (Figure 2). Maximum settlement of the crest surface was about 8.0 cm (Figure 3), and main three cracks attained about 2.0 - 3.0 m depth were observed around the top edge of downstream slope (Figure 4).

Azuma Dam is a fill-type dam with mudstone and central clay core zone shown in Figure 11 completed 1971. It is 38.2 m high and 222.0 m long, impounding up to 10,080,000 m^3 of water. Two seismometers were installed at the crest and the base ground as shown in Figure 11. Azuma Dam also located around the epicenter of this earthquake and the recorded base peak acceleration obtained by the seismometer in upstream and downstream direction was 297 Gal, and 1293 Gal was recorded at the dam crest (Figure 12). The recorded

DOI: 10.1201/9781003299127-169

acceleration lasted only 30 seconds because the power supply was lost due to the slope failure on the right side downstream of the dam embankment. Maximum settlement of the crest surface was about 14.9 cm (Figure 13).

A simple strain softening elasto-plastic constitutive model is rather robust for application to a dynamic response analysis of fill-type dams. This strain softening material model was applied to Mizuho Dam and Azuma Dam with the features of non-associated flow characteristics, post-peak strain softening and strain-localization into a shear band with a specific width. In order to avoid the numerical instability due to the singularity of non-associated Mohr-Coulomb model, the constitutive model based on the yield function of Mohr-Coulomb type and the plastic potential function of Drucker-Prager type were used.

2 MATERIAL MODEL FOR BEHAXIOR OF GEOMATERIALS

The material model will be briefly described in this section (Tanaka 2002, 2015). The yield function (f) and the plastic potential function (Φ) are given by:

$$f = \alpha I_1 + \frac{\bar{\sigma}}{g(\theta_L)} - K = 0 \tag{1}$$

$$\Phi = \alpha' I_1 + \bar{\sigma} - K = 0 \tag{2}$$

where

$$\alpha = \frac{2\sin\phi}{\sqrt{3}(3-\sin\phi)} \tag{3}$$

$$K = \frac{6c\cos\phi}{\sqrt{3}(3-\sin\phi)} \tag{4}$$

$$\alpha' = \frac{2sin\psi}{\sqrt{3}(3-sin\psi)} \tag{5}$$

$$\sin\psi = \frac{\sin\phi - \sin\phi'_R}{1-\sin\phi\sin\phi'_R} \tag{6}$$

where I_1 is the first invariant (positive in tension) of deviatoric stresses and $\bar{\sigma}$ is the second invariant of deviatoric stress. With the Mohr-Coulomb model, $g(\theta_L)$ takes the following form;

$$g(\theta_L) = \frac{3-\sin\phi}{2\sqrt{3}\cos\theta_L - 2\sin\theta_L\sin\phi} \tag{7}$$

ϕ is the mobilized friction angle, c is the cohesion, ψ is the dilatancy angle and θ_L is the Lode angle.

In case of simple strain softening constitutive model, the frictional softening is given by next function.

$$\alpha(\kappa) = \alpha_p + \alpha_1\kappa/(B+\kappa) \;\; \alpha_1 = -(\alpha_p - \alpha_R) \tag{8}$$

and cohesion softening function is by next function.

$$\gamma(\kappa) = \gamma_p + \gamma_1\kappa/(C+\kappa) \;\; \gamma_1 = -(\gamma_p - \gamma_R) \tag{9}$$

The dilatancy is reduced by next function.

$$\alpha'(\kappa) = \alpha'_p(1 - \kappa/(C + \kappa)) \tag{10}$$

where κ is plastic parameter, B, C, D are constants for softening function. The suffices P, R represent the peak and residual state. Where γ is shear strain, γ_R is reference shear strain.

A more realistic frictional softening functions expressed as follows;

$$\alpha(\kappa) = \alpha_r + (\alpha_p - \alpha_r)\exp\left\{-\left(\frac{\kappa - \varepsilon_f}{\varepsilon_r}\right)^2\right\} \quad (\kappa \geq \varepsilon_f) \tag{11}$$

where ε_f and ε_r are the material constants and α_p and α_r are the values of α at the peak and residual states.

The residual friction angle (ϕ_r) and Poison's ratio (ν) were chosen based on the data from the triaxial compression test.

$$G_0 = G_E \frac{(2.17 - e)^2}{1 + e}\sigma_m^{0.4} \tag{12}$$

The elastic moduli are estimated using the following equations.

$$K = \frac{2(1 + \nu)}{3(1 - 2\nu)}G \tag{13}$$

The peak friction angle is a function of confining pressure, initial void ratio e and G_E is empirical constant.. The dilatancy angle (ψ) was estimated from Rowe's stress-dilatancy relation. The introduction of shear banding in the numerical analysis was achieved by introducing a strain localization parameter s in the following additive decomposition of total strain increment as follows.

$$d\varepsilon_{ij} = d\varepsilon^e_{ij} + sd\varepsilon^p_{ij} \quad s = F_b/F_e \tag{14}$$

where F_b is the area of a single shear band in each element and F_e is the area of the element.

An one-point integration method and an hourglass control scheme are used with 4-noded two-dimensional isoparametric element (Flanagan & Belytschko 1979). This element is effective and suited for collapse analysis of frictional material with shear banding. The most fully integrated continuum elements tend to lock especially for geomaterials, so the selection of element type is important for the collapse analyses of embankment dams. Simple shear strength is appropriate for earthquake response analysis of a fill-type dam and triaxial compression test results of layered soil sample are approximately equivalent to shear strength of horizontally anisotropic fill materials. We employed the triaxial compression test results for the two-dimentional dynamic analyses of fill-type dams.

3 DYNAMIC RESPONSE ANALYSIS OF MIZUHO DAM

The simple strain softening elasto-plastic constitutive equation was applied to the impounded Mizuho Dam. Figure 5 showed the finite element mesh used for dynamic response analysis. Before dynamic response analysis, build-up analysis was carried out.

Table 1 showed the material parameters for the dynamic analysis. The core materials (①, ②) were assumed undrained condition during the earthquake and elasto-plastic constitutive

model was applied. The strengths of core materials were obtained by isotropically consolidated undrained triaxial compression test. The internal friction angle was 25.3°. The cohesion was 32.3 kN/m^2. The constant (G_E) for elastic moduli was 40,000 kN/m^2. The assumed shear band thickness (*S.B.*) was 0.5 cm, taking into consideration that the thickness of shear band is 15~20 times of mean diameter of fill materials.

The strengths of semi-permeable materials were obtained by isotropically consolidated undrained triaxial compression test combined with cyclic loading and succeeding monotonic loading. The material constants of these zones used for the analyses were as follows: φ_{peak} = 32.0°, φ_{res} = 24.6°, c_{peak} = 53.0 kN/m^2, c_{res} = 38.8 kN/m^2, B = 0.5, C = 0.3, D = 0.7, G_E = 80,000 kN/m^2, *S.B.* = 3.0 cm (Case 1).

For semi-permeable zones (④, ⑥, ⑩) mainly at downstream slope side, drained condition were assumed. The strengths of semi-permeable materials were obtained by isotropically consolidated drained triaxial compression tests. The material constants of these zones were as follows: φ_{peak} = 39.2°, φ_{res} = 36.1°, c_{peak} = 22.0 kN/m^2, c_{res} = 19.0 kN/m^2, B = 0.5, C = 0.3, D = 0.7, G_E = 80,000 kN/m^2, *S.B.* = 3.0 cm (Case 2).

The filter zone (⑦) was assumed drained condition and the material constants of this zone are as follows: φ_{peak} = 42.9°, φ_{res} = 33.0°, c_{peak} = c_{res} = 0.0 kN/m^2, B = 0.5, C = 0.3, G_E = 100,000 kN/m^2, *S.B.* = 5.0 cm. The riprap (⑧, ⑨) zones were assumed drained conditions and the material constants of these zone were as follows: φ_{peak} = 44.0°, φ_{res} = 33.0°, c_{peak} = c_{res} = 0.0 kN/m^2, B = 0.5, C = 0.3, G_E = 120,000 kN/m^2, *S.B.* = 14.0 cm.

The Rayleigh damping was assumed 5.0%. The input acceleration was measured one at the base of dam as shown in Figure 2.

In Case 1, Figure 6 showed the computed response acceleration at the crest centre. Although the computed maximum response acceleration was larger than measured maximum response acceleration (937 Gal), the time of computed maximum response acceleration agreed at the time (12 second) of measured maximum response acceleration. Figure 7 showed the computed vertical displacements around crest. Maximum vertical displacements of No.2812 at the crest center and No.2785 around the top edge of upstream slope were about 5.0 cm, and maximum vertical displacements of No.2823 around the top edge of downstream slope was about 7.0 cm. As the measured crest settlements of this dam were within ranging from 5.3cm to 8.0cm, we could say that the comparable results were obtained.

In Case 2, Figure 8 showed the computed response acceleration at the crest center. The computed maximum response acceleration of Case 2 was smaller than that of Case 1, and the time of maximum acceleration agreed well as Case 1. Figure 9 showed the computed vertical displacement around crest. Although results of Case 2 tended to be larger than those of Case 1, the comparable result was obtained in Case 2, too.

Figure 10 showed the computed maximum shear strain distributions after 40 sec. by Case 1 and Case 2. The computed maximum shear strain (Case 1), was about 13% and concentrated around the top edge of downstream slope as shown in Figure 10, so we could say that the comparable results as observed were obtained.

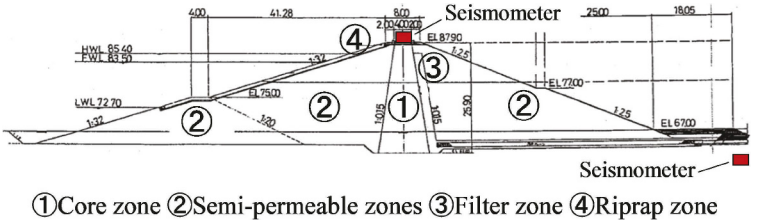

Figure 1. Cross section of Mizuho Dam.

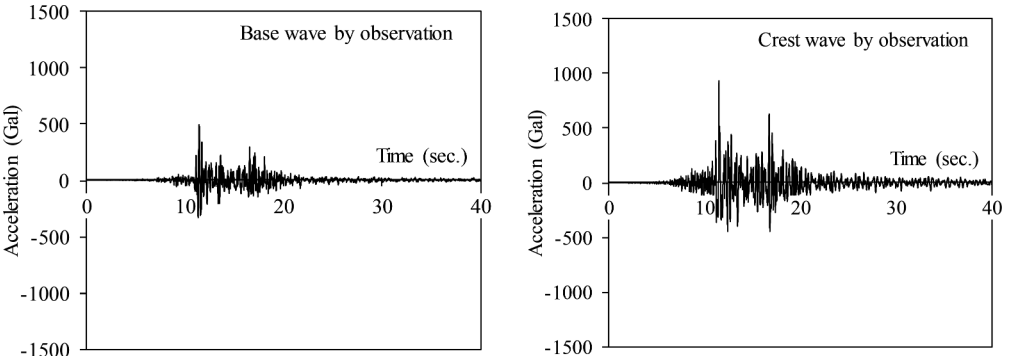

Figure 2. Measured acceleration at the base and crest of Mizuho Dam.

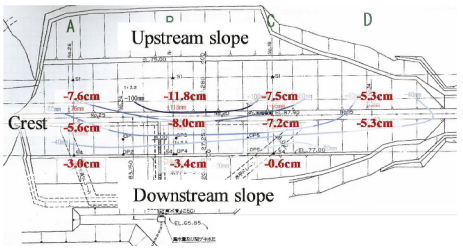

Figure 3. Settlements of crest surface in Mizuho Dam.

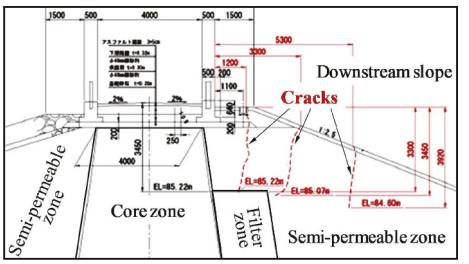

Figure 4. Three major cracks at down stream slope in Mizuho Dam.

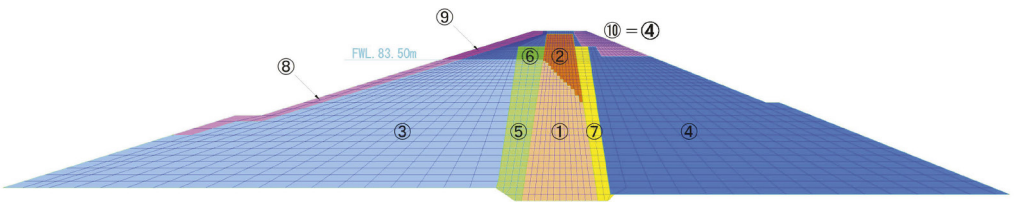

Figure 5. Finite element mesh of Mizuho Dam.
(Total number f elements:2727, Total number of nodes:2835)

Table 1. Material parameters for simple strain softening elasto-plastic analysis.

Material No.	Material name	γ (kN/m3)	φ_{peak} (degree)	φ_{res} (degree)	C_{peak} (kN/m2)	C_{res} (kN/m2)	G_E (kN/m2)	*S.B.* (cm)
①	Core (Saturation)	19.2	25.3	25.3	32.3	32.3	40,000	0.5
②	Core (Un-saturation)	18.7	25.3	25.3	32.3	32.3	40,000	0.5
③=⑤	Semi-permeable (Saturation)	21.4	32.0	24.6	53.0	38.8	80,000	3.0
④=⑤ =⑩	Semi-permeable (Un-saturation)	18.7	32.0 (39.2)	24.6 (36.1)	53.0 (22.0)	38.8 (19.0)	80,000	3.0
⑦	Filter (Un-saturation)	22.7	42.9	33.0	0.0	0.0	100,000	5.0
⑧	Riprap (Saturation)	22.7	44.0	33.0	0.0	0.0	100,000	14.0
⑨	Riprap (Un-saturation)	22.7	44.0	33.0	0.0	0.0	120,000	14.0

The figures in parentheses are obtained by consolidated drained test (CD-test)

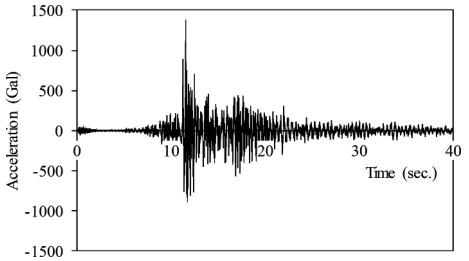

Figure 6. Computed response acceleration at the center crest (Case 1).

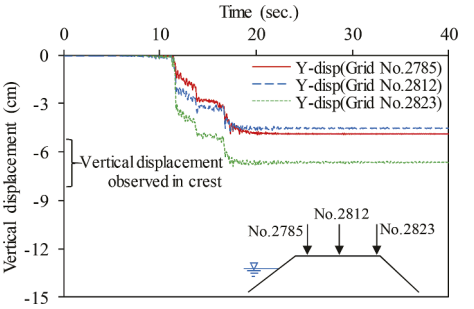

Figure 7. Computed displacements around crest (Case 1).

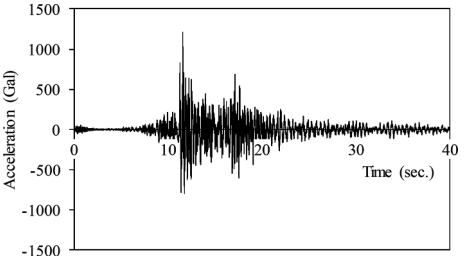

Figure 8. Computed response acceleration at the center of crest (Case 2).

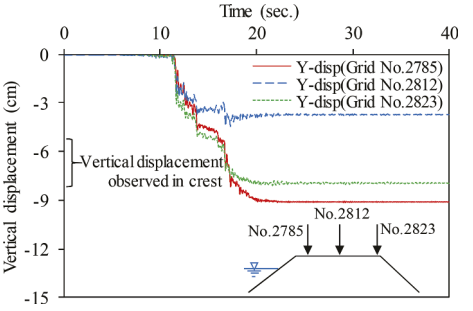

Figure 9. Computed displacement around crest (Case 2).

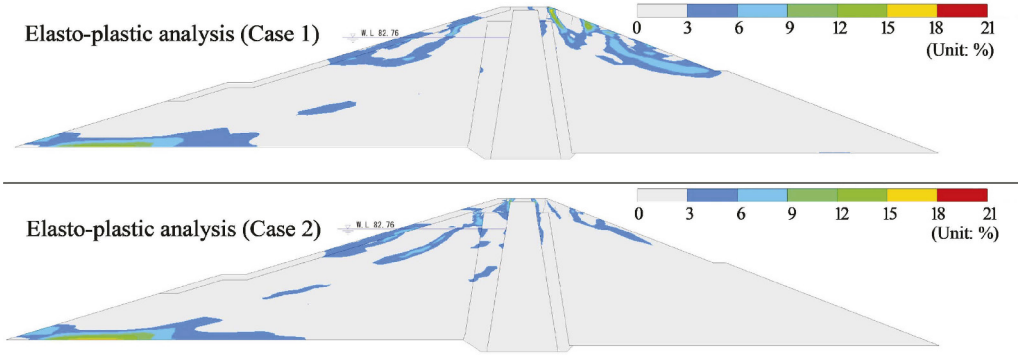

Figure 10. Computed maximum shear strain distributions in 40 second.

4 DYNAMIC RESPONSE ANALYSIS OF AZUMA DAM

The simple strain softening elasto-plastic constitutive equation was also applied to the impounded Azuma Dam. Figure 14 showed the finite element mesh used for dynamic response analysis. Before dynamic response analysis, build-up analysis was carried out.

Table 2 shows material parameters for the dynamic analysis. The Core1 (①, ②) and Core2 (③) materials were assumed undrained condition during the earthquake. The total stress

strengths of core materials were obtained by isotropically consolidated undrained triaxial compression test. The Core1 internal friction angle was 15.0° and cohesion was 37 kN/m^2. The Core2 internal friction angle was 13.0° and cohesion was 51 kN/m^2. The elastic moduli (G_E) were 40,000 kN/m^2. The assumed shear band thickness (S.B.) was 0.2 cm.

The semi-permeable zones (④, ⑥) were assumed undrained condition during the earthquake. The total stress strengths of semi-permeable materials were obtained by isotropically consolidated undrained triaxial compression test. The material constants of saturated semi-permeable zones (④, ⑥) used for strain softening model were as follows: φ_{peak} = 15.0°, φ_{res} = 15.0°, c_{peak} = 81.5 kN/m^2, c_{res} = 81.5 kN/m^2, B = 0.5, C = 0.3, D = 0.7, G_E = 80,000 kN/m^2, S.B. = 4.0 cm. For unsaturated semi-permeable zones (⑤) at downstream slope side, the strengths of the material was obtained by isotropically consolidated undrained triaxial test on the in-situ density (density of 100% D-value). The material constants of this zone were as follows: φ_{peak} = 27.2°, φ_{res} = 27.2°, c_{peak} = 7.4 kN/m^2, c_{res} = 7.4 kN/m^2, B = 0.5, C = 0.3, D = 0.7, G_E = 80,000 kN/m^2, S.B. = 4.0 cm.

The filter zone (⑦, ⑧) was assumed drained condition and the material constants of this zone as follows: φ_{peak} = 40°, φ_{res} = 40°, c_{peak} = c_{res} = 0.0 kN/m^2, B = 0.5, C = 0.3, G_E = 100,000 kN/m^2, S.B. = 1.8 cm. The riprap (⑨, ⑩) zone was assumed drained condition and the material constants of this zone were as follows: φ_{peak} = 30°, φ_{res} = 30°, c_{peak} = c_{res} = 0.0 kN/m^2, B = 0.5, C = 0.3, G_E = 120,000 kN/m^2, S.B. = 20 cm.

The Rayleigh damping was assumed 5.0%. The input acceleration was measured one at the base of dam as shown in Figure 12. Figure 15 showed the computed response acceleration at the crest centre by simple strain softening elasto-plastic analysis. Although the computed maximum response acceleration (1090 Gal) was smaller than measured maximum response acceleration (1293 Gal), the time of computed maximum response acceleration agreed with the time (15.6 second) of measured maximum response acceleration. Figure 16 showed the computed vertical displacements the around crest by simple strain softening elasto-plastic analysis. The maximum vertical displacements of No.1809 at the crest center and No.1814 around the top edge of downstream slope were about 5.4 cm and 8.6 cm. Maximum vertical displacements of No.1805 around the top edge of upstream slope was about 18.1 cm. As the maximum measured crest settlement of this dam was within ranging from 14.9 cm, we could say that the comparable results were obtained.

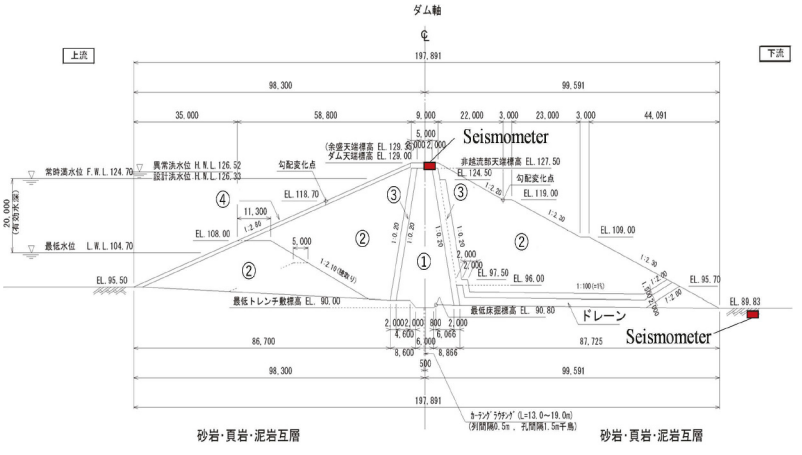

①Core zone ②Semi-permeable mudstone zone ③Filter zone ④Riprap zone

Figure 11. Cross section of Azuma Dam.

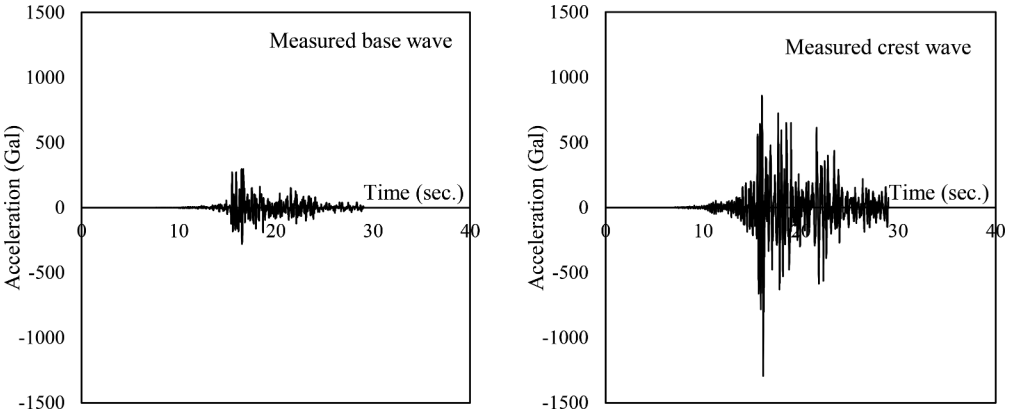

Figure 12. Measured acceleration at the base and the crest of Azuma Dam.

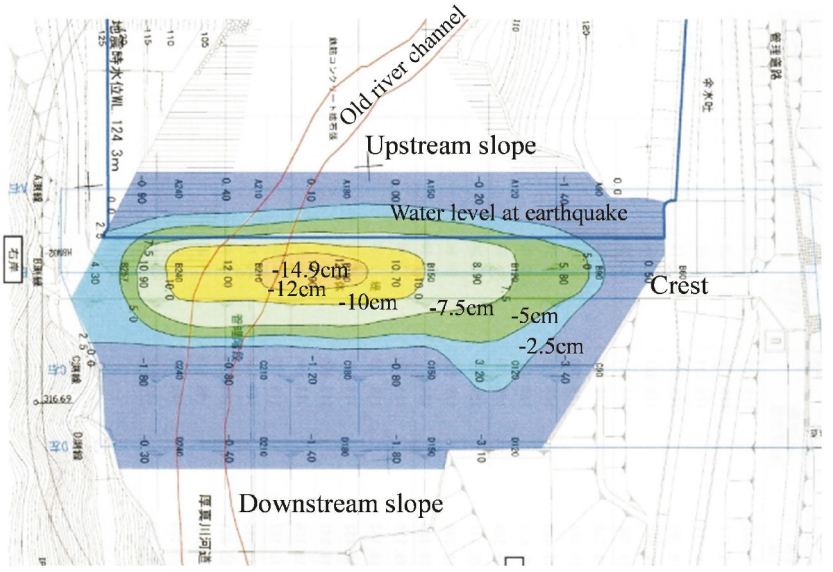

Figure 13. Measured surface settlements of Azuma Dam.

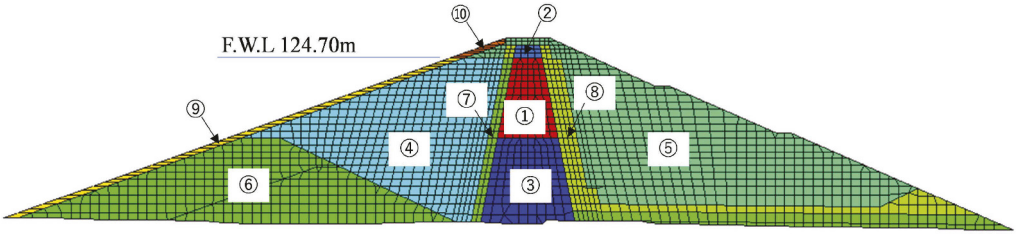

Figure 14. Finite element mesh of Azuma Dam.
(Total number of elements:1761, Total number of nodes:1814).

Table 2. Material parameters for simple strain softening elasto-plastic analysis.

Material No.	Material name	γ kN/m3	φ_{peak} degree	φ_{res} degree	C_{peak} kN/m2	C_{res} kN/m2	G_E kN/m2	S.B. cm
①	Core1 (Saturation)	20.6	15	15	37	37	40,000	0.2
②	Core1 (Un-saturation)	20.3	15	15	37	37	40,000	0.2
③	Core2 (Saturation)	20.7	13	13	51	51	40,000	0.2
④=⑥	Semi-permeable (Saturation)	21.4	15	15	81.5	81.5	80,000	4
⑤	Semi-permeable (Saturation)	20.3	27.2	27.2	7.4	7.4	80,000	4
⑦	Filter (Saturation)	21.1	40	40	0	0	100,000	1.8
⑧	Filter (Saturation)	21	40	40	0	0	100,000	1.8
⑨	Riprap (Saturation)	19.6	30	30	0	0	120,000	20
⑩	Riprap (Saturation)	17.3	30	30	0	0	120,000	20

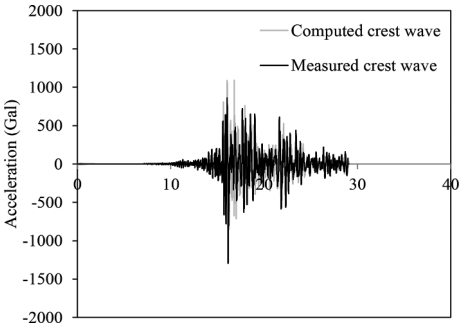

Figure 15. Computed response acceleration at the center of crest.

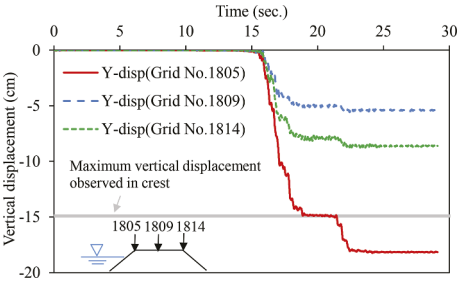

Figure 16. Computed displacements around crest.

5 CONCLUSIONS

A simple strain softening material model for geomaterial is used with the features of post-peak strain softening, and strain-localization into a shear band with a specific width. This material model is applied to the computation of real rock-fill dams. We obtained earthquake induced accelerations and displacements of Mizuho Dam which is 25.9 m high and Azuma Dam which is 38.2 m high. The computed accelerations at the crest of dams are compared to the observed ones and the computed displacements are also verified by the observed displacements. The simple strain softening constitutive model is applicable to the computation of a real fill-type dam.

REFERENCES

Flanagan, D.P. & Belytschko, T. 1979. A uniform strain hexahedron and quadrilateral with orthgonal hourglass control, *Int. J. Numer. Methods Eng.*, Vol.14, 679–706.

Tanaka, T. 2002. Elasto-plastic strain hardening-softening soil model with shear banding. *Proc. 15th ASCE Engineering Mechanics Conf.*, New York, p.8 (CD-ROM).

Tanaka, T. 2015. Cyclic behavior of soils and numerical analyses in cold regions and seismic zones. *Sciences in Cold and Arid Regions*, Vol.7 Issue 5, 492–502.